(2)

AD-A223 065

OFFICE OF NAVAL RESEARCH

Contract N00014-87-J-1118

R & T Code 4133016

Technical Report No. 15

Adsorption of Pyridine at the Au(110) - Solution Interface

by

L. Stolberg, J. Lipkowski, and D.E. Irish

Prepared for Publication

in

Journal of Electroanalytical Chemistry

Guelph-Waterloo Center for Graduate Work in Chemistry
Waterloo, Campus
Department of Chemistry
University of Waterloo
Waterloo, Ontario
Canada, N2L 3G1

May 28, 1990

SECURITY CLASSIFICATION OF THIS PAGE

REPORT DOCUMENTATION PAGE

1a REPORT SECURITY CLASSIFICATION Unclassified	1b RESTRICTIVE MARKINGS
2a SECURITY CLASSIFICATION AUTHORITY Unclassified	3 DISTRIBUTION / AVAILABILITY OF REPORT Public Release/Unlimited
2b DECLASSIFICATION / DOWNGRADING SCHEDULE	
4 PERFORMING ORGANIZATION REPORT NUMBER(S) ONR Technical Report #15	5 MONITORING ORGANIZATION REPORT NUMBER(S)
6a NAME OF PERFORMING ORGANIZATION D. E. Irish University of Waterloo 6b OFFICE SYMBOL (If applicable)	7a NAME OF MONITORING ORGANIZATION Office of Naval Research
6c ADDRESS (City, State, and ZIP Code) Department of Chemistry University of Waterloo Waterloo, Ontario, Canada, N2L 3G1	7b ADDRESS (City, State, and ZIP Code) The Ohio State University, Research Center 1314 Kinnear Road, Room 318 Columbus, Ohio, U.S.A., 43212-1194
8a NAME OF FUNDING / SPONSORING ORGANIZATION Office of Naval Research 8b OFFICE SYMBOL (If applicable)	9 PROCUREMENT INSTRUMENT IDENTIFICATION NUMBER N00014-87-J-1118
8c ADDRESS (City, State, and ZIP Code) Chemistry Division 800 N. Quincy Street Arlington, VA, U.S.A., 22217-5000	10 SOURCE OF FUNDING NUMBERS PROGRAM ELEMENT NO / PROJECT NO / TASK NO / WORK UNIT ACCESSION NO

11 TITLE (Include Security Classification)

Adsorption of Pyridine at the Au(110) - Solution Interface

12 PERSONAL AUTHOR(S)
L. Stolberg, J. Lipkowski, and D.E. Irish

13a TYPE OF REPORT	13b TIME COVERED	14 DATE OF REPORT (Year, Month, Day)	15 PAGE COUNT
Technical	FROM 05/89 TO 05/89	1990-05-28	37

16 SUPPLEMENTARY NOTATION

Submitted to Journal of Electroanalytical Chemistry

17 COSATI CODES			18 SUBJECT TERMS (Continue on reverse if necessary and identify by block number)
FIELD	GROUP	SUB-GROUP	Pyridine adsorption; single crystal gold surface; Au(110); orientation of pyridine on gold surfaces; surface coverage

19 ABSTRACT (Continue on reverse if necessary and identify by block number)

The energetics of pyridine adsorption onto a Au(110) surface have been characterized quantitatively using chronocoulometry. The adsorption parameters such as relative Gibbs surface excesses, Gibbs energies of adsorption, and electrosorption valencies have been determined as a function of the electrode potential and the surface-charge density. The maximum surface excess is equal to 6.1×10^{-10} mol cm^{-2}, the Gibbs energy at the potential of maximum adsorption is -42 kJ mol^{-1}, and the shift of the potential of zero charge (pzc) due to displacement of a monolayer of water molecules by a monolayer of adsorbed pyridine is -0.65 V. It is concluded that pyridine molecules are adsorbed vertically on a Au(110) surface, attached to the metal by the nonbonding orbital of the nitrogen atom. Adsorption of pyridine at Au(110) and Au(100) surfaces are compared. The strong effect of surface crystallography on the energetics of pyridine adsorption at gold electrodes is shown.

20 DISTRIBUTION / AVAILABILITY OF ABSTRACT ☒ UNCLASSIFIED/UNLIMITED ☐ SAME AS RPT. ☐ DTIC USERS	21 ABSTRACT SECURITY CLASSIFICATION Unclassified
22a NAME OF RESPONSIBLE INDIVIDUAL Dr. Robert J. Nowak	22b TELEPHONE (Include Area Code) (519) 885-1211, ext. 2500 22c OFFICE SYMBOL

DD FORM 1473, 84 MAR 83 APR edition may be used until exhausted. All other editions are obsolete.

SECURITY CLASSIFICATION OF THIS PAGE
Unclassified

ADSORPTION OF PYRIDINE AT THE Au(110) - SOLUTION INTERFACE

L. Stolberg[1,2], J. Lipkowski[1] and D.E. Irish[2]

Guelph-Waterloo Centre for Graduate Work in Chemistry
[1]Department of Chemistry and Biochemistry
University of Guelph
Guelph, Ontario, Canada N1G 2W1

[2]Department of Chemistry
University of Waterloo
Waterloo, Ontario, Canada N2L 3G1

Abstract

The energetics of pyridine adsorption onto a Au(110) surface have been characterized quantitatively using chronocoulometry. The adsorption parameters such as relative Gibbs surface excesses, Gibbs energies of adsorption, and electrosorption valencies have been determined as a function of the electrode potential and the surface-charge density. The maximum surface excess is equal to 6.1×10^{-10} mol cm^{-2}, the Gibbs energy at the potential of maximum adsorption is -42 kJ mol^{-1}, and the shift of the potential of zero charge (pzc) due to displacement of a monolayer of water molecules by a monolayer of adsorbed pyridine is -0.65 V. It is concluded that pyridine molecules are adsorbed vertically on a Au(110) surface, attached to the metal by the nonbonding orbital of the nitrogen atom. Adsorption of pyridine at Au(110) and Au(100) surfaces are compared. The strong effect of surface crystallography on the energetics of pyridine adsorption at gold electrodes is shown.

Introduction

This is the third paper in a series devoted to the study of the effect of crystallographic orientation of gold electrodes on the adsorption of pyridine. In two previous contributions the adsorption of pyridine at the polycrystalline [1] and Au(100) surface [2] have been described. In this communication, results of investigations of pyridine adsorption onto the Au(110) surface will be presented and quantitative data such as adsorption isotherms, Gibbs energies of adsorption and electrosorption valencies will be given. The orientation of pyridine molecules adsorbed at the Au(110) surface has been determined and the differences between the adsorption at Au(110) and Au(100) are discussed. The very strong effect of surface crystallography on pyridine adsorption at gold surfaces is reported.

Experimental

Experimental procedures used in this work have been described in preceding communications [1-4]. The working electrode was a gold(110) single crystal rod (99.99%,

Johnson Matthey). Before each experiment the working electrode was flamed and then quenched with Milli-Q water. Kolb and Schneider [5] have shown, using LEED and RHEED, that the Au(110) electrode surface, which has been prepared by the flame treatment method, exhibits a (1 x 2) superstructure. In a later work Zei et al. [6] found, from combined LEED and electrochemical experiments, that the Au(110) - (1 x 2) structure is stable in 0.01 M $HClO_4$ solution up to a potential of about +0.9 V (SCE). More positive polarizations lift the reconstruction irreversibly. Therefore, in our work, a potential sweep up to +1.2 V (SCE) upper limit was applied just after the contact between the electrode and the electrolyte was made, in order to lift the reconstruction. Consequently, in view of Kolb's results, all our experiments were performed with the surface having the (1 x 1) structure.

The instrumentation and sequence of different steps involved in the data acquisition and processing have been described in previous papers. The experimental strategy involved characterization of the surface by cyclic voltammograms and differential capacity curves and quantitative determination of the electrode charge density, σ_M, from chronocoulometric experiments [1-4]. The charge density data were then used to calculate relative Gibbs excesses and free energies of adsorption.

All solutions were prepared from Milli-Q Water (Waters). The supporting electrolyte was 0.1 M $KClO_4$. All solutions were deaerated with argon and during the experiment argon was passed over the top of the solution. The experiments were carried out at 25 $\pm$ 1°C. Potentials were measured with respect to the external saturated calomel reference electrode (SCE).

Results

(i) Cyclic Voltammetry

Shown in Fig. 1 are two cyclic voltammograms which have been recorded in the absence and presence of pyridine, Figures 1a and 1b, respectively. It was always found that cyclic voltammograms which superimpose from one cycle to the next could be obtained after 3 to 5

cycles recorded immediately after contact between the crystal and the electrolyte was made. No distortion of the curves due to the creeping effect or the presence of oxygen could be detected, provided the concentration of pyridine $\leq 6 \times 10^{-4}$ M. These observations suggest that the solutions investigated were always of high purity and free of oxygen.

The cyclic voltammogram recorded for the supporting electrolyte shows that the double layer region extends from -0.8 V to +0.6 V. For electrode potentials more negative than -0.8 V hydrogen evolution on Au(110) begins. For potentials more positive than +0.6 V oxidation of the gold surface takes place, as Figure 1a shows. This immediately suggests that pyridine adsorption studies on Au(110) will be restricted to the potential region -0.8 V to +0.6 V.

The oxide formation region of the cyclic voltammogram for the supporting electrolyte displays four features. This is in good agreement with the data reported by Lecoeur [7] for Au(110) in the presence of 0.02 M NaF. On the reverse, negative scan, three peaks can be distinguished. The most positive peak was not observed by Lecoeur. The differences between the present results and Lecoeur's can be explained by the different experimental conditions used in the two studies. Lecoeur worked in a 0.02 M NaF solution (pH 6.5) and stirred the solution during his experiments. We worked in a 0.1 M $KClO_4$ solution and did not stir. Fig. 1b shows that several changes to the cyclic voltammogram take place upon the addition of pyridine. In the double layer region pyridine adsorption/desorption peaks are visible. These features can be seen for pyridine concentrations as low as 10^{-5} M. The addition of pyridine has not affected the extent of the double layer region which can still be defined by the potential limits -0.8 V to +0.6 V. In the oxide formation region only one main peak can be seen with a shoulder present on the cathodic side. The effect of pyridine on the structure of the cyclic voltammogram in this region could be seen for a concentration of pyridine as low as 2×10^{-6} M.

Integration of the positive branches of the cyclic voltammograms obtained in the absence and presence of pyridine for potentials greater than +0.6 V showed that the charge is

1.17 times greater when pyridine is present in the solution. This may indicate that the pyridine molecules are being partially oxidized at the Au(110) electrode surface. The negative branches of the cyclic voltammograms were also integrated. The charges were found to be equal for solutions with and without pyridine. This shows that the same amount of oxide was deposited in the positive half of the cycle for the two cases and that pyridine oxidation is irreversible.

Cyclic voltammetry has shown that for electrode potentials more negative than -0.8 V hydrogen evolution takes place. Also, for potentials more positive than +0.6 V oxidation of the gold electrode surface begins. It was found that for pyridine concentrations > 6×10^{-4} M the electrolyte started to creep onto the walls of the Au(110) electrode. Therefore pyridine adsorption studies were restricted to the potential region -0.8 V to +0.6 V and to pyridine concentrations $\leq 6 \times 10^{-4}$ M.

(ii) Differential Capacity

Differential capacity curves which were obtained for the Au(110) single crystal electrode, both in the absence and presence of pyridine, are shown in Fig. 2. The data presented here correspond to a potential sweep of 5 mV s^{-1} in the positive direction. The curve for the supporting electrolyte (0.1 M $KClO_4$) displays two capacitance peaks at -0.25 V and +0.23 V. The capacitance peak at +0.23 V has a slightly higher value than that which occurs at -0.25 V. Qualitatively, this curve is in good agreement with the differential capacity curve reported by Hamelin [8] for Au(110) in the presence of 0.01 M NaF. These data are also in good agreement with those of Nguyen et al. [9] and Lecoeur [7] who have also reported differential capacity curves for the Au(110) electrode.

The minimum which appears on the differential capacity curve shown in Fig. 2 for the supporting electrolyte gives the potential of zero charge (pzc) as -0.015 V in 0.1 M $KClO_4$. This value for the pzc is in reasonable agreement with the value of -0.06 V reported by Lecoeur [7] in

NaF. This difference may be attributed to the different anions of the supporting electrolyte present in the two cases. Perchlorate adsorbs less strongly then fluoride and therefore a more positive pzc is observed.

The differential capacity curves for Au(110) in the presence of 3×10^{-5} M, 10^{-4} M and 6×10^{-4} M pyridine show only one capacitance peak, seen at negative electrode potentials. This peak is observed to shift in the direction of negative potentials and its height increases as the bulk pyridine concentration increases. This capacitance peak is characteristic of adsorption/desorption of pyridine. For the 3×10^{-5} M and 10^{-4} M solutions, the capacity peak displays a shoulder on the anodic side while the curve for the 6×10^{-4} M pyridine solution displays a shoulder on the cathodic side of the peak. For the most negative potentials shown in Fig. 2, the capacity curves for the various pyridine concentrations merge with the capacity curve for the supporting electrolyte. This behaviour suggests that in this region of potentials the pyridine molecules are completely desorbed from the Au(110) electrode surface. For the most positive potentials shown the capacity curves reach a minimum value and merge with one another.

Hamelin [10] was the first to report differential capacity curves for pyridine adsorption onto Au(110) using 0.2 M K_2SO_4 as the supporting electrolyte. The data which were presented for Au(110) in the presence of 1.23×10^{-4} M pyridine are very similar to the capacity curve shown in Fig. 2 for the 10^{-4} M pyridine solution in the region of the capacity peak. However, the shoulder which appears on the anodic side of the capacity peak is absent from the differential capacity curve reported by Hamelin. The differences can be attributed to different supporting electrolytes used in the two studies.

(iii) Charge-Potential Plots

Step experiments were carried out in order to obtain quantitative data for the adsorption process. The electrode was initially held at a potential (initial potential) at which

pyridine adsorption takes place for a period of time long enough to establish a state of equilibrium between the interface and the bulk of the solution (approximately 2 min.). Then, the potential was stepped to the value E = -0.8 V (final potential) at which a total desorption of pyridine takes place (see Fig. 2) and the current transient corresponding to the charging of the interface was recorded. The charging current was subsequently integrated and the absolute charge density, σ_M, at the initial potential was calculated using the procedure described in ref. [1-3].

Presented in Fig. 3 are the absolute charge density-potential plots which were obtained for the Au(110) electrode in both the presence and absence of pyridine. Pyridine concentrations ranging from 2 x 10^{-6} M to 6 x 10^{-4} M are shown in this figure. The reproducibility of the charge data was checked and found to be very good (better than 1%). For the most extreme negative electrode potentials shown in Fig. 3, the σ_M versus E plots for the various pyridine concentrations are seen to merge with the σ_M - E curve obtained for the supporting electrolyte. This correspondence of charge shows that the pyridine molecules are desorbed from the Au(110) electrode surface. This result is consistent with the differential capacitance measurements presented in Fig. 2. Beyond this region the data display a strong dependence on the bulk pyridine concentration. The charge density curves display an initial fast rising section followed by a quasi-plateau. For pyridine concentrations $\geq 10^{-5}$ M the curves merge with one another in the plateau region and σ_M becomes independent of the pyridine concentration in the bulk of the solution. This behaviour indicates that the surface concentration of pyridine reached a maximum (saturation) value Γ_{max}. Linear extrapolation of the initial segment of the plateau section of the curve to $\sigma_M = 0$ allowed the determination of the shift of the potential of zero charge, E_N, which results from the displacement of a monolayer of water molecules from the electrode surface by a monolayer of adsorbed pyridine. With the help of Fig. 3 a value of E_N corresponding to -0.65 V has been determined. The value of E_N is large and negative and we will show later that this indicates that the pyridine

molecules are oriented with the nitrogen facing the metal and the hydrocarbon part facing the solution side of the interface.

The section of the σ_M versus E curve for which σ_M is independent of the bulk pyridine concentration is seen to intersect the curve of the supporting electrolyte approximately at a potential of +0.23 V or at a charge of +24 μC cm^{-2}. These values correspond to the potential and charge of maximum adsorption, respectively. The curves corresponding to the two lowest concentrations intersect the supporting electrolyte plot at a slightly more positive potential and higher charge densities, indicating that E_{max} and σ_{max} depend slightly on the bulk pyridine concentration.

(iv) Film and Surface Pressure Curves

The film and surface pressures (π and ϕ, respectively) have been calculated from the charge density data using the back integration procedure described in ref. [3].

Shown in Figure 4 are the film pressure versus electrode potential curves for the various pyridine concentrations investigated. All the plots presented in Fig. 4 are bell shaped and display a well defined maximum. For the three lowest pyridine concentrations the maximum shows a small positive shift which was observed earlier on the charge density graphs. Fig. 5 shows the ϕ versus σ_M curves for the various pyridine solutions investigated. The analysis at a constant charge density has been restricted to charges smaller than +20 μC cm^{-2}. (Note that a charge density of +20 μC cm^{-2} corresponds to a potential of approximately +0.1 V.) Because only a limited range of charge densities have been examined the maximum which was displayed on the π vs. E curves cannot be seen on the surface pressure plots. However, the curves shown in Fig. 5 clearly have a bell-shaped appearance.

Both the film and surface pressure reach fairly large values (> 80 mN m^{-1}) for an electrode surface which is positively charged and for moderate to high pyridine concentrations.

This shows that the zero coverage Gibbs energy of adsorption and/or energy of lateral interactions between adsorbed pyridine molecules are large.

(v) Adsorption Isotherms

The relative Gibbs surface excesses were initially determined by differentiation of the film pressure versus logarithm of the bulk pyridine concentration curves. The lateral interactions between adsorbed pyridine molecules are relatively strong and hence the π versus ln(c) plots displayed a relatively sharp bend at low film pressures followed by a linear segment. The error of differentiation in the bent region was large. Therefore, the values of Γ were calculated directly from the σ_M data using the formula:

$$\Gamma = \frac{\sigma_{M,\Gamma} - \sigma_{M,\Gamma=0}}{\sigma_{M,\Gamma_{max}} - \sigma_{M,\Gamma=0}} \Gamma_{max} \qquad (1)$$

where values of Γ_{max} were determined from the slope of the linear segments of π versus ln(c) plots. The agreement between the values of Γ determined by the two methods was generally good.

The relative Gibbs excesses are plotted against the electrode potential for the various pyridine concentrations studied in Fig. 6. Presented in Fig. 7 are the plots of Γ versus ln(c) (adsorption isotherms) determined at a constant electrode potential. The curves span the region -0.45 V to -0.1 V. For electrode potentials more negative than -0.35 V, only fragments of the isotherm could be obtained due to the limited range of bulk pyridine concentrations studied. The curves shown in Figs. 5 and 7 have sigmoidal shape with only one inflection point and a well defined plateau. This type of behaviour suggests that the pyridine molecules assume only one orientation at the Au(110) surface. The limiting surface concentration is equal to 6.1×10^{-10} mol cm^{-2} and this value is consistent with the vertical orientation of the

pyridine molecules. This result is in full agreement with the large shift of the potential of zero charge in the negative direction reported earlier.

The relative Gibbs surface excess was also evaluated by graphical differentiation of the surface pressure versus the natural logarithm of the bulk pyridine concentration curves using σ_M as the independent electrical variable. The results, Γ versus σ_M and Γ versus ln(c), are presented in Figs. 8 and 9, respectively. In excellent agreement with the analysis carried out using potential as the electrical variable is the value of Γ_{max} which was found to be 6.2×10^{-10} mol cm^{-2}. Overall, the values of Γ determined from the analysis at constant charge agree reasonably well with those determined from the analysis at constant electrode potential. However, qualitative differences between the adsorption isotherms determined at constant electrode potential and constant charge exist. Comparing Figs. 7 and 9 one can see that the Γ versus ln(c) curves determined at constant electrode potential display only one inflection point while those determined at constant charge display two. In addition, the isotherms presented in Fig. 7 are steep indicating attractive lateral interactions while those shown in Fig. 9 are tilted suggesting repulsive lateral interactions.

(vi) Gibbs Energy of Adsorption

The Gibbs energy of adsorption was determined from the initial slopes of π versus bulk pyridine concentration plots using the expression for the Henry's Law isotherm as explained in ref. [2]. The value of $\Gamma_{max} = 6.1 \times 10^{-10}$ mol cm^{-2} was used in the calculations.

In addition the equation of the Frumkin isotherm was fitted to the data presented in Fig. 7:

$$\beta c = \frac{\theta}{1 - \theta} \exp A\theta \qquad (2)$$

where β is the adsorption coefficient, related to the Gibbs energy of adsorption through

$$\Delta G^{\circ} = -RT\ln \beta \qquad (3)$$

$\theta = \Gamma/\Gamma_{max}$ and A is the so called lateral interaction parameter. A good fit to equation 2 was achieved with the parameter A weakly dependent on the electrode potential (A varied from a value of -3.5 at E = -0.3 V to -2.0 at E = +0.05 V).

The values of Gibbs energies of adsorption determined by both methods are plotted in Fig. 10. They correspond to the standard state being unit mole fraction of pyridine in the bulk of the solution and unit coverage at the surface (unsymmetrical choice of the standard state [11]). The agreement between the values of ΔG° determined by the two methods is fully satisfactory, indicating that the data are free from major systematic errors. The dependence of ΔG° on potential has a quasi parabolic shape with maximum centered at E_{max} = +0.225 V which is in good agreement with the value of E_{max} determined earlier with the help of charge-density-potential plots.

The first derivative of ΔG° versus E is equal to the electrosorption valency γ'. The electrosorption valency can also be determined from the dependence of the charge density on the surface concentration of pyridine at constant electrode potential using the following relationship [12]:

$$\gamma' = \frac{1}{F}\left(\frac{\partial \mu_p}{\partial E}\right)_{\Gamma} = \left(\frac{1}{F}\right)\left(\frac{\partial \Delta G^{\circ}}{\partial E}\right)_{\Gamma} = -\frac{1}{F}\left(\frac{\partial \sigma_M}{\partial \Gamma}\right)_E \qquad (4)$$

The slopes of σ_M versus Γ plots can then be compared to the first derivative of ΔG° versus E plots and used in this way to check the consistency of our results.

Shown in Fig. 11 are plots of σ_M versus Γ for various electrode potentials in the region from -0.40 to +0.10 V. Straight line relationships are observed over the entire range of electrode potentials presented. The slopes of these lines allow the evaluation of the electrosorption valency. The values of γ' which were determined from the data presented in

Fig. 11 were plotted as a function of the electrode potential in Fig. 12. Independently, the ΔG° versus E data determined from the Henry's Law isotherm were fitted by a polynominal of the 4th order and numerically differentiated. The electrosorption valencies determined by the differentiation of the Gibbs energy data are also plotted in Fig. 12. The agreement between the two sets of data is very good and indicates that our results are self consistent.

The Gibbs energies of adsorption were also determined from the initial slopes of the surface pressure versus bulk pyridine concentration plots using charge density as the independent electrical variable. The values of ΔG° are plotted against σ_M in Fig. 13. The data display a pseudo parabolic dependence on the electrode charge density with the maximum value of ΔG° approximately equal to -42 kJ mol^{-1} in good agreement with the value of ΔG°_{max} determined from analysis based on potential as the independent electrical variable.

By cross differentiation of the elecrocapillary equation one can find that:

$$(\partial E/\partial \Gamma)\sigma_M = (\partial \Delta G/\partial \sigma_M)_{\Gamma} \qquad (5)$$

Therefore the first derivative of the Gibbs energy of adsorption with respect to the charge density should be equal to the slope of the electrode potential versus the surface excess plot taken at a constant charge density. The electrode potential E is related to $\Delta_2{}^M\phi$, the potential drop across the inner layer, by

$$\Delta_2{}^M\phi = E - E_{pzc} - \phi_2 \qquad (6)$$

where E_{pzc} is the potential of zero charge and ϕ_2 is the potential drop across the diffuse layer obtained from Gouy-Chapman theory. A plot of $\Delta_2{}^M\phi$ versus Γ at constant charge densities is shown in Fig. 14. The plots are nonlinear; however, the limiting slopes of these curves taken at $\Gamma \rightarrow 0$ progressively decrease with negative charge at the surface. The initial slopes of these curves are compared to the result of the numerical differentiation of the ΔG° versus σ_M curve in Fig. 15. Although the scatter of the experimental points is large, satisfactory agreement

between the two sets of data is observed indicating that no major errors were made in the data processing.

Summary and Conclusions

The data have been presented using both the potential and the charge density as the independent electrical variable. We do not claim any preference with respect to the choice of the electrical variable. The basic adsorption parameters characterizing pyridine adsorption at the Au(110) surface are summarized and compared with the data for the Au(100) plane in Table 1. The Gibbs energy of adsorption is large and indicates that a strong specific interaction takes place between the pyridine molecules and the gold surfaces.

The displacement of a monolayer of water by a monolayer of adsorbed pyridine molecules shifts the potential of zero charge by -0.65 V. Using a simple electrostatic model, the potential difference across the inner region of the double layer can be given by [13, 14]:

$$\Delta_2{}^M\phi = (\sigma_M x_2 + \Gamma\bar{\mu})/\epsilon \qquad (7)$$

and the shift of pzc can be expressed as:

$$E_N = \Gamma_{max}(\bar{\mu}/\epsilon) \qquad (8)$$

where $\bar{\mu}$ is the effective dipole moment equal to

$$\bar{\mu} = \bar{\mu}^{org} - n\bar{\mu}^w \qquad (9)$$

$\bar{\mu}^i$ is the component of the dipole moment perpendicular to the gold surface, i stands for the organic and water molecules, respectively, n is the number of water dipoles replaced at the surface by one pyridine molecule, ϵ and x_2 are the dielectric constant and thickness of the inner layer, respectively.

Apparently a large negative value of E_N indicates that $\bar{\mu}$ is large and negative. This strongly suggests that the pyridine molecules are oriented with the negative pole of their dipole moment facing the metal [2]. The maximum of the Gibbs excess corresponds to an area for one molecule of 0.27 nm^2 which is very close to the value of 0.25 nm^2 found for a vertically adsorbed pyridine molecule [15]. In summary, the magnitudes of $\Delta G^{\bullet}_{max}$, E_N and Γ_{max} strongly suggests that the pyridine molecules are adsorbed vertically at the Au(110) surface with the nitrogen atom facing the metal and the hydrocarbon part directed toward the solution side of the interface. Very similar results for pyridine adsorption at the Ag(110) electrode have been obtained recently in our laboratory [16]. Also it has been reported that the pyridine molecules assume the vertical orientation at the (110) plane of Cu, Ag and Au when adsorbed at the bare surface of these metals from gas phase [17-19].

The $\Delta_2{}^M\,\phi$ versus Γ plots shown in Fig. 14 are nonlinear. In view of the electrostatic model, equation 7, the nonlinearity indicates that either $\bar{\mu}/\varepsilon$ and/or x_2/ε vary with Γ. At zero charge density equation 7 simplifies to:

$$\Delta_2{}^M\,\phi \;=\; \Gamma(\bar{\mu}/\varepsilon) \qquad (10)$$

The plot of $\Delta_2{}^M\phi$ versus Γ at $\sigma_M = 0$ displays a weak curvature indicating that although $(\bar{\mu}/\varepsilon)$ changes slightly with coverage the deviations from linearity are small. Such behaviour suggests that no significant reorientation of the adsorbed molecules takes place at the gold surface investigated. This conclusion is supported by the shapes of adsorption isotherms shown in Fig. 7 which display only one inflection point.

The electrostatic model can be explored further to give a molecular interpretation to the dependence of the Gibbs energy of adsorption on the electrical variable. By differentiation of equation 7 with respect to Γ at a constant σ_M one can obtain:

$$(\partial\Delta_2{}^M\phi/\partial\Gamma)\sigma_M \;=\; \sigma_M\partial(x_2/\varepsilon)/\partial\Gamma \;+\; \bar{\mu}/\varepsilon \qquad (11)$$

In a similar way we can express the electrosorption valency γ' in terms of:

$$\gamma' = -\{\Delta_2{}^M\phi\partial(\varepsilon/x_2)/\partial\Gamma + \bar{\mu}/x_2\}/F \qquad (12)$$

In the limit of low surface coverages, ε and x_2 should be approximately equal to the values observed in a pure solvent. Consequently, the first term of equations 11 and 12 should be independent of the electrical variable. If we further assume that $\bar{\mu}^{org}$ does not change with E or σ_M, then the dependence of γ' on E shown in Fig. 12 and the dependence of $(\partial\Delta_2{}^M\phi/\partial\Gamma)\sigma_M$ on σ_M shown in Fig. 15 illustrate the variation of the dipole moment of the solvent $\bar{\mu}^w$ as a function of the electrical variable. In fact the plots presented in Fig. 12 and Fig. 15 have quite similar shape. Apparently the dependence of the effective dipole moment for water on E or σ_M is nonlinear. Such deviations from linearity can in principle be predicted from molecular models proposed by Guidelli et al. [20]. In conclusion, the dependence of the Gibbs energy of adsorption on the electrical variable is, to a large extent, determined by the changes of the effective dipole moment for the solvent and hence by the magnitude of the gold-water interactions.

There are significant differences between adsorption of pyridine at the Au(110) and Au(100) surfaces. As we reported earlier [2] the pyridine molecules assume a flat orientation at the negatively and the vertical orientation at the positively charged Au(100) plane. In contrast only one orientation is observed at the Au(110) surface. Consequently, the pyridine molecule behaves as a bidentate ligand coordinating either through π-orbitals of the aromatic ring or through the nonbonding orbital localized at the nitrogen atom to the Au(100) surface and as a monodentate ligand, attached only through the nonbonding orbital to the Au(110) face. There are also quantitative differences between the energetics of pyridine adsorption in the vertical orientation at the two surfaces of gold, illustrated by the adsorption parameters presented in Table 1 and by the comparison of adsorption isotherms for 10^{-4} M pyridine solutions shown in Fig. 16. The upper part of the isotherms corresponds to a vertical orientation of the molecules

at the two surfaces. The isotherm for the Au(110) surface is shifted by about 0.35 V in the negative direction with respect to the curve for the Au(100) plane. This is to be compared with only a 0.16 V difference between the values of pzc for the two planes. The adsorption of pyridine at the Au(110) surface must be, therefore, much stronger than at the Au(100) plane. In conclusion, surface crystallography has a significant effect on pyridine adsorption at Au electrodes. We will discuss this point in more detail in the next publication in which the adsorption data for other crystallographic orientations will be presented.

Acknowledgements

This work was supported by grants from the Natural Sciences and Engineering Research Council of Canada and the Office of Naval Research (U.S.A.)

Literature

1. L. Stolberg, J. Richer, J. Lipkowski, and D.E. Irish, J. Electroanal. Chem., 207 (1986) 213.

2. L. Stolberg, J. Lipkowski, and D.E. Irish, J. Electroanal. Chem., 238 (1987) 333.

3. J. Richer and J. Lipkowski, J. Electrochem. Soc., 133 (1986) 121.

4. J. Richer, L. Stolberg, and J. Lipkowski, Langmuir, 2 (1986) 630.

5. D.M. Kolb and J. Schneider, Electrochimica. Acta, 31 (1986) 929.

6. M.S. Zei, G. Lehmpfuhl, and D.M. Kolb, Surface Sci., 221 (1989) 23.

7. J. Lecoeur, Thesis, University of Paris 1979.

8. A. Hamelin, in B.E. Conway, R.E. White, and J.O'M. Bockris (Eds.) Modern Aspects of Electrochemistry, Vol. 16, Plenum Press, New York, 1985, p. 1.

9. C. Nguyen van Huong, C. Hinnen, J. Lecoeur, and R. Parsons, J. Electroanal. Chem., 92 (1978) 239.

10. (a) A. Hamelin and G. Valette, C.R. Acad. Sci., Ser. C, 267 (1968) 211.

    (b) A. Hamelin, J. Electroanal. Chem., 144 (1983) 365.

11. (a) D.M. Mohilner, H. Nakadomari, and P. Mohilner, J. Phys. Chem., 81 (1977) 244.

    (b) J. Jastrzebska, M. Jurkiewicz-Herbich, and S. Trasatti, J. Electroanal. Chem., 216 (1987) 21.

12. K.J. Vetter and J.W. Schultze, Ber. Bunsenges. Phys. Chem., 76 (1972) 920.

13. R. Parsons, Trans. Faraday Soc., 55 (1959) 999.

14. R. Parsons, J. Electroanal. Chem., 7 (1964) 136.

15. B.E. Conway, J.G. Mathieson, and H.P. Dhar, J. Phys. Chem., 78 (1974) 1226.

16. A. Hamelin, S. Morin, J. Richer, and J. Lipkowski, J. Electroanal. Chem., 272 (1989) 241.

17. K.H. Frank, R. Dudde, and E.E. Koch, Chem. Phys. Letters, 132 (1986) 83.

18. (a) A. Otto, K.H. Frank, and B. Reihl, Surf. Sci., 163 (1985) 140.

    (b) A. Otto, K.H. Frank, and B. Reihl, Surf. Sci., 162 (1985) 891.

19. R. Dudde, K.H. Frank, M.L.M. Rocco, and E.E. Koch, Surf. Sci., 201 (1988) 469.

20. R. Guidelli, In Trends in Interfacial Electrochemistry, Silva, A.F. Ed.; NATO ASI Series C, 1986, Vol. 179, p. 387.

Legend to Figures

Fig. 1 Cyclic voltammogram recorded for (a) 0.1 M $KClO_4$ and (b) 0.1 M $KClO_4$ + 6 x 10^{-4} M pyridine. Sweep rate 20 mV s^{-1}, electrode area -0.0654 cm^2.

Fig. 2 Differential capacity curves for (-·-·-) 0.1 M $KClO_4$, (———) 0.1 M $KClO_4$ + 3 x 10^{-5} M pyridine, (·····) 0.1 M $KClO_4$ + 10^{-4} M pyridine and (----) 0.1 M $KClO_4$ + 6 x 10^{-4} M pyridine. Sweep rate 5 mV s^{-1}, and the ac modulating frequency 25 Hz with an amplitude of 5 mV rms.

Fig. 3 Charge density - potential curves determined for the following pyridine concentrations: (▲) 0; (■) 2 x 10^{-6} M; (Δ) 5 x 10^{-6} M; (○) 10^{-5} M; (*) 3 x 10^{-5} M; (●) 7 x 10^{-5} M; (X) 10^{-4}; (□) 3 x 10^{-4} M; (■) 6 x 10^{-4} M. Supporting electrolyte 0.1 M $KClO_4$.

Fig. 4 Film pressure curves for the following pyridine concentrations: (1) 2 x 10^{-6} M; (2) 5 x 10^{-6} M; (3) 7 x 10^{-6} M; (4) 10^{-5} M; (5) 3 x 10^{-5} M; (6) 7 x 10^{-5} M; (7) 10^{-4} M; (8) 3 x 10^{-4} M; (9) 6 x 10^{-4} M. $\pi = \gamma_{\theta=0} - \gamma_\theta$; γ is the interfacial tension and indices $\theta = 0$ and θ denote the interface free from and covered by adsorbed pyridine molecules.

Fig. 5 Surface pressure curves for the following pyridine concentrations: (◊) 2 x 10^{-6} M; (▼) 5 x 10^{-6} M; (∇) 7 x 10^{-6} M; (■) 10^{-5} M; (□) 3 x 10^{-5} M; (▲) 7 x 10^{-5} M; (Δ) 10^{-4} M; (●) 3 x 10^{-4} M; (○) 6 x 10^{-4} M. $\phi = \xi_{\theta=0} - \xi_\theta$; $\xi = \gamma + \sigma_M E$ is the Parson's function and indices θ=0 and θ denote the interface free from and covered by adsorbed pyridine molecules.

Fig. 6 Surface concentration - potential curves for the following bulk pyridine concentrations: (1) 2 x 10^{-6} M; (2) 5 x 10^{-6} M; (3) 7 x 10^{-6} M; (4) 10^{-5} M; (5) 3 x 10^{-5} M; (6) 7 x 10^{-5} M; (7) 10^{-4} M; (8) 3 x 10^{-4} M; (9) 6 x 10^{-4} M.

Fig. 7 Adsorption isotherms which have been obtained at the following electrode potentials: (1) -0.45 V; (2) -0.40 V; (3) -0.35 V; (4) -0.30 V; (5) -0.25 V; (6) -0.20 V; (7) -0.15 V; (8) -0.10 V. C is the bulk pyridine concentration.

Fig. 8 Surface concentrations - electrode charge density curves obtained for the following bulk pyridine concentrations: (1) 2×10^{-6} M; (2) 5×10^{-6} M; (3) 7×10^{-6} M; (4) 10^{-5} M; (5) 3×10^{-5} M (6) 7×10^{-5} M; (7) 10^{-4} M; (8) 3×10^{-4} M; (9) 6×10^{-4} M.

Fig. 9 Adsorption isotherms determined at constant charge densities, the values of which in $\mu C\ cm^{-2}$ is indicated at the corresponding curve.

Fig. 10 Plot of ΔG° versus E as determined from the Henry's Law isotherm, filled circles, and from a fit to the equation of the Frumkin isotherm - open circles.

Fig. 11 Plots of σ_M versus Γ at constant E. (0) -0.40 V; (●) -0.30 V; (□) -0.25 V; (■) -0.20 V; (Δ) -0.15 V; (▲) -0.10 V; (◊) -0.05 V; (♦) 0 V; (▽) +0.05 V; (▼) +0.10 V.

Fig. 12 Comparison of the electrosorption valencies determined from (0), the slopes of the σ_M versus Γ plots, and (❑) by numerical differentiation of the ΔG° vs. E curve corresponding to Henry's Law.

Fig. 13 Plot of ΔG° versus σ_M determined from the Henry's Law isotherm.

Fig. 14 Plot of $\Delta_2{}^M\phi$ versus Γ for the various charge densities indicated.

Fig. 15 Comparison of the dependence of $(\partial\Delta_2{}^M\phi/\partial\Gamma)\sigma_M$ on the charge density determined from the initial slopes of the plots in Fig. 14, open circles, and by the numerical differentiation of the Gibbs energy with respect to the electrode charge density, filled squares.

Fig. 16 Comparison of the isotherms for pyridine adsorption at Au(110) and Au(100) surfaces from 10^{-4} M pyridine solution.

Table 1

Adsorption Parameters for Pyridine Adsorption on the Au(110) and Au(100) Surfaces

Parameter	Au(110)	Au(100)	
		Flat	Vertical
$(E_{max}-E_{pzc})/V$	0.25	-0.09	0.26
$\sigma_{max}/\mu C\ cm^{-2}$	24	-4	+34
E_N/V	-0.65	+0.02	-0.8
$\Delta G^{\circ}_{max}/k\ J\ mol^{-1}$	-42	-36	-
$10^{10}\ \Gamma_{max}/mol\ cm^{-2}$	6.1	assumed 3	6
E_{pzc}/V vs. SCE	-0.015	+0.14	+0.14

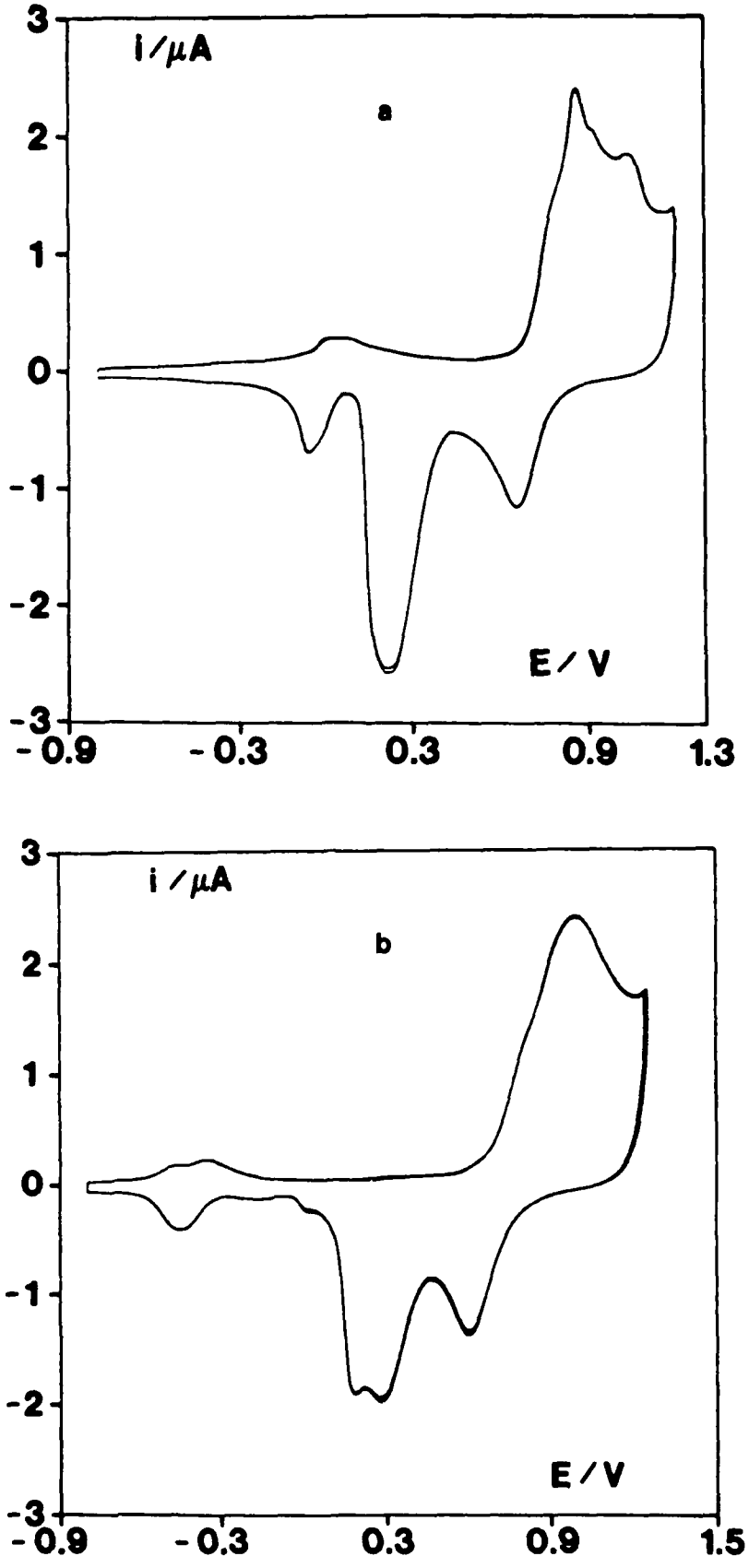

Fig. 1 Cyclic voltammogram recorded for (a) 0.1 M $KClO_4$ and (b) 0.1 M $KClO_4$ + 6 x 10^{-4} M pyridine. Sweep rate 20 mV s^{-1}, electrode area -0.0654 cm^2.

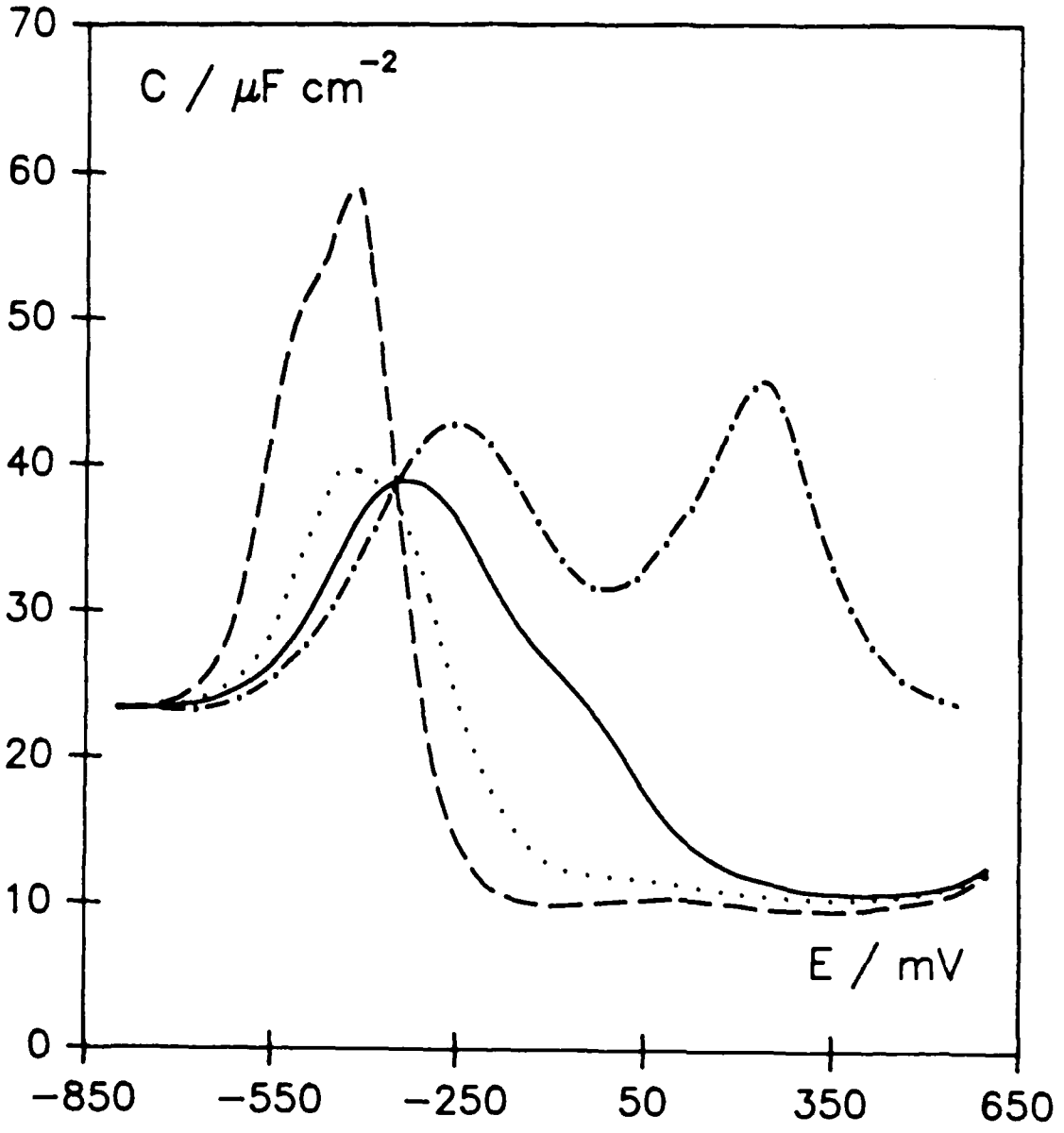

Fig. 2 Differential capacity curves for (·····) 0.1 M $KClO_4$, (———) 0.1 M $KClO_4$ + 3 x 10^{-5} M pyridine, (·····) 0.1 M $KClO_4$ + 10^{-4} M pyridine and (----) 0.1 M $KClO_4$ + 6 x 10^{-4} M pyridine. Sweep rate 5 mV s^{-1}, and the ac modulating frequency 25 Hz with an amplitude of 5 mV rms.

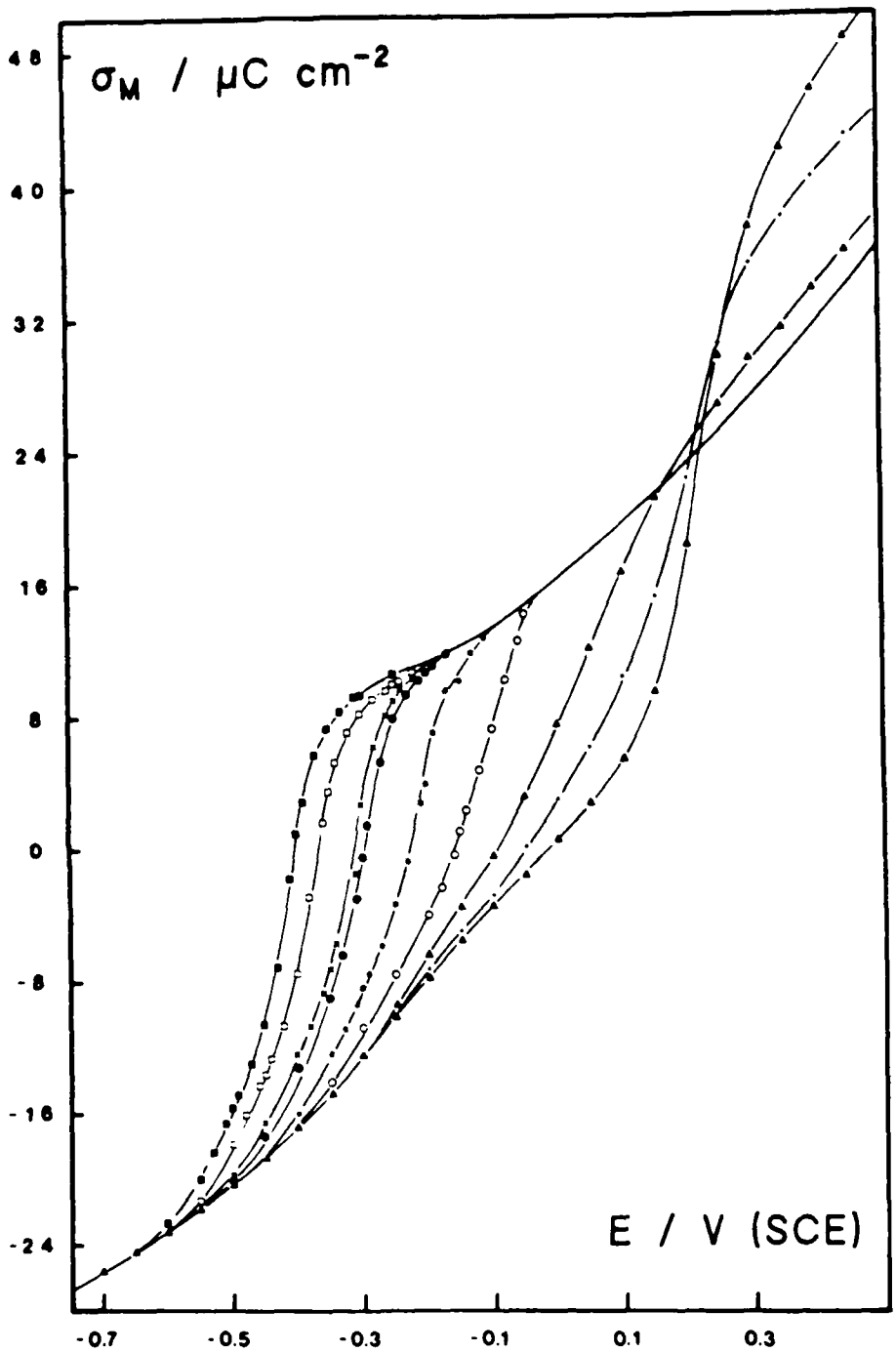

Fig. 3 Charge density - potential curves determined for the following pyridine concentrations: (▲) 0; (▪) 2 x 10^{-6} M; (Δ) 5 x 10^{-6} M; (○) 10^{-5} M; (•) 3 x 10^{-5} M; (●) 7 x 10^{-5} M; (X) 10^{-4}; (□) 3 x 10^{-4} M; (■) 6 x 10^{-4} M. Supporting electrolyte 0.1 M $KClO_4$.

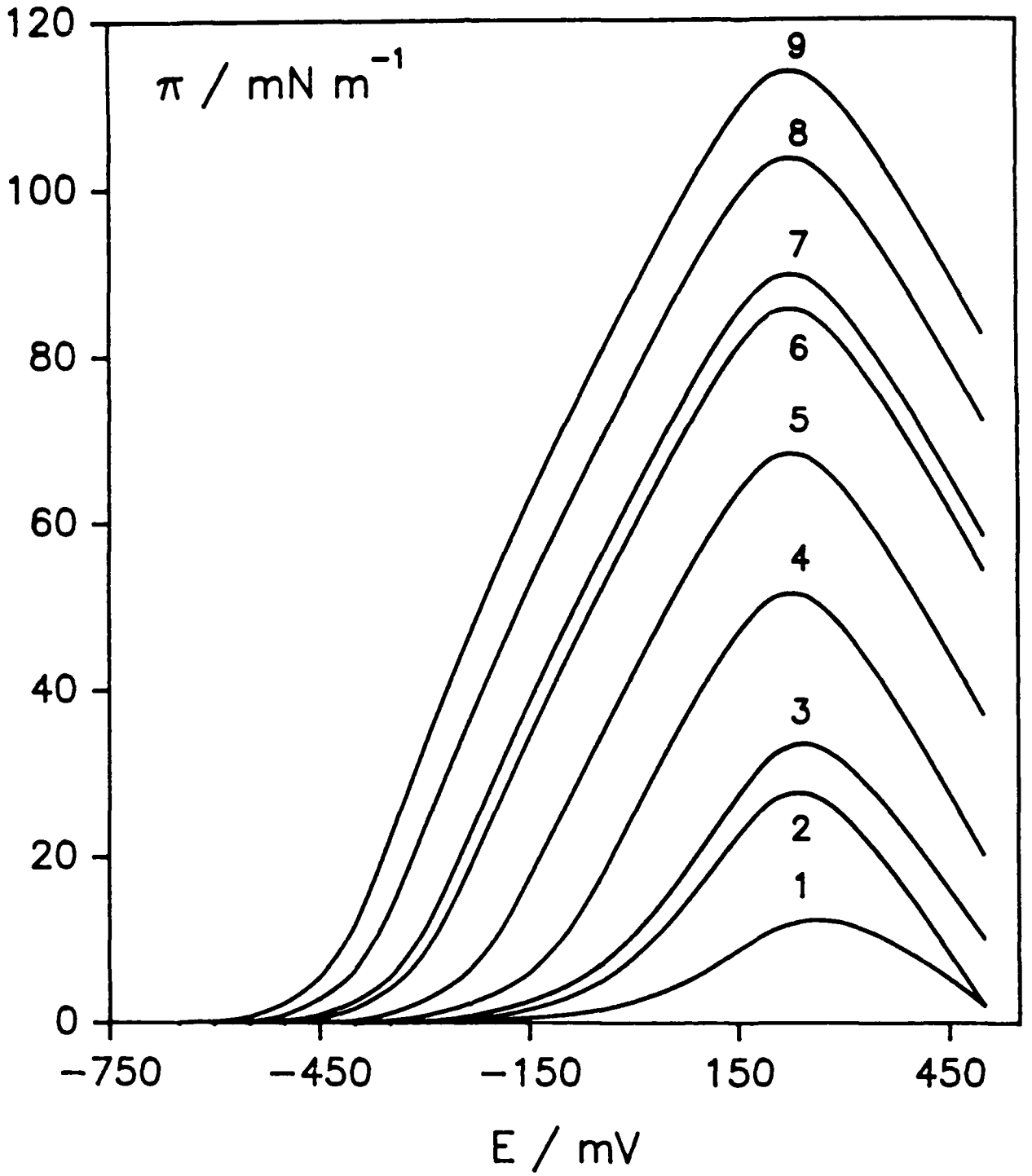

Fig. 4 Film pressure curves for the following pyridine concentrations: (1) 2 x 10^{-6} M; (2) 5 x 10^{-6} M; (3) 7 x 10^{-6} M; (4) 10^{-5} M; (5) 3 x 10^{-5} M; (6) 7 x 10^{-5} M; (7) 10^{-4} M; (8) 3 x 10^{-4} M; (9) 6 x 10^{-4} M. $\pi = \gamma_{\theta=0} - \gamma_{\theta}$; γ is the interfacial tension and indices $\theta = 0$ and θ denote the interface free from and covered by adsorbed pyridine molecules.

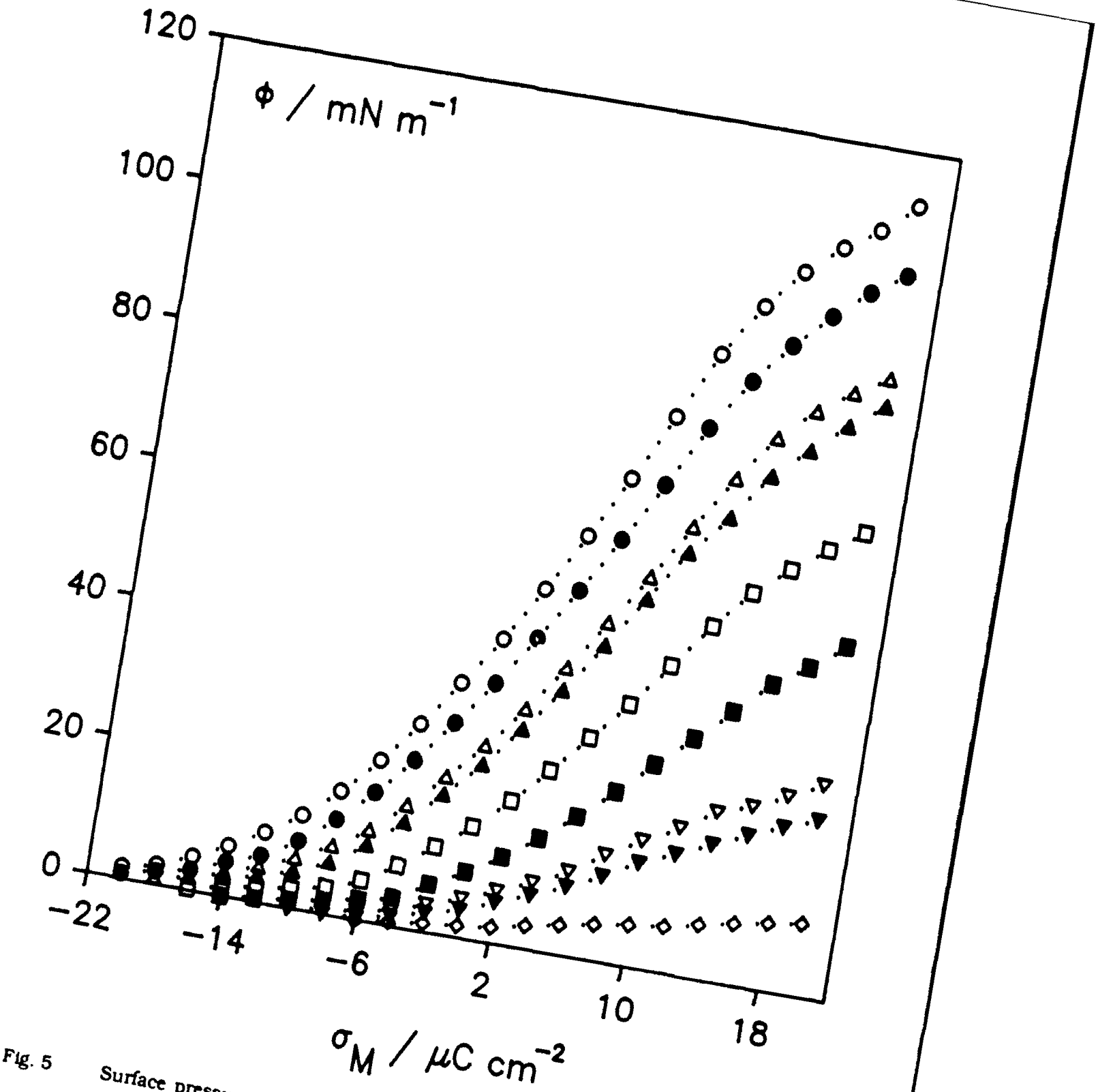

Fig. 5 Surface pressure curves for the following pyridine concentrations: (◊) 2×10^{-6} M; (▼) 5×10^{-6} M; (▽) 7×10^{-6} M; (■) 10^{-5} M; (□) 3×10^{-5} M; (▲) 7×10^{-5} M; (△) 10^{-4} M; (●) 3×10^{-4} M; (○) 6×10^{-4} M. $\phi = \xi_{\theta=0} - \xi_{\theta}$; $\xi = \gamma + \sigma_M E$ is the Parson's function and indices $\theta=0$ and θ denote the interface free from and covered by adsorbed pyridine molecules.

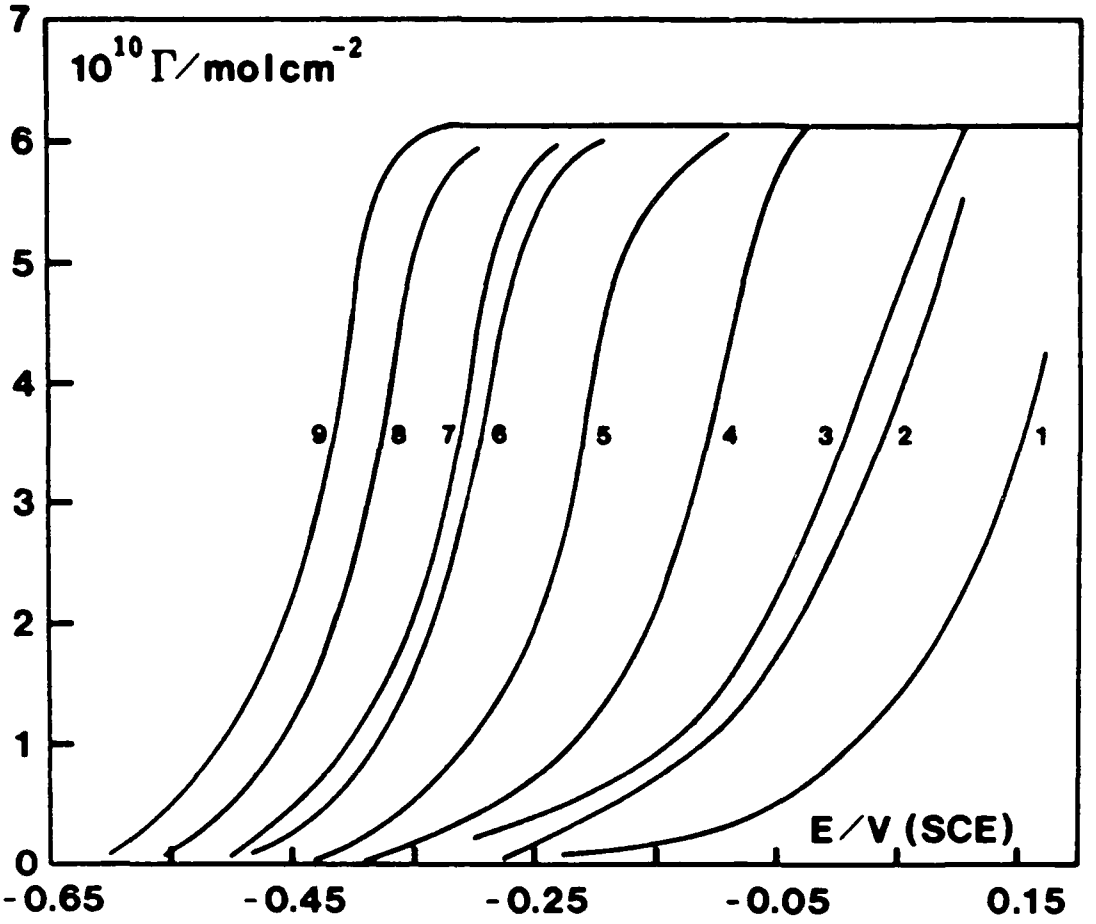

Fig. 6 Surface concentration - potential curves for the following bulk pyridine concentrations: (1) 2 x 10^{-6} M; (2) 5 x 10^{-6} M; (3) 7 x 10^{-6} M; (4) 10^{-5} M; (5) 3 x 10^{-5} M; (6) 7 x 10^{-5} M; (7) 10^{-4} M; (8) 3 x 10^{-4} M; (9) 6 x 10^{-4} M.

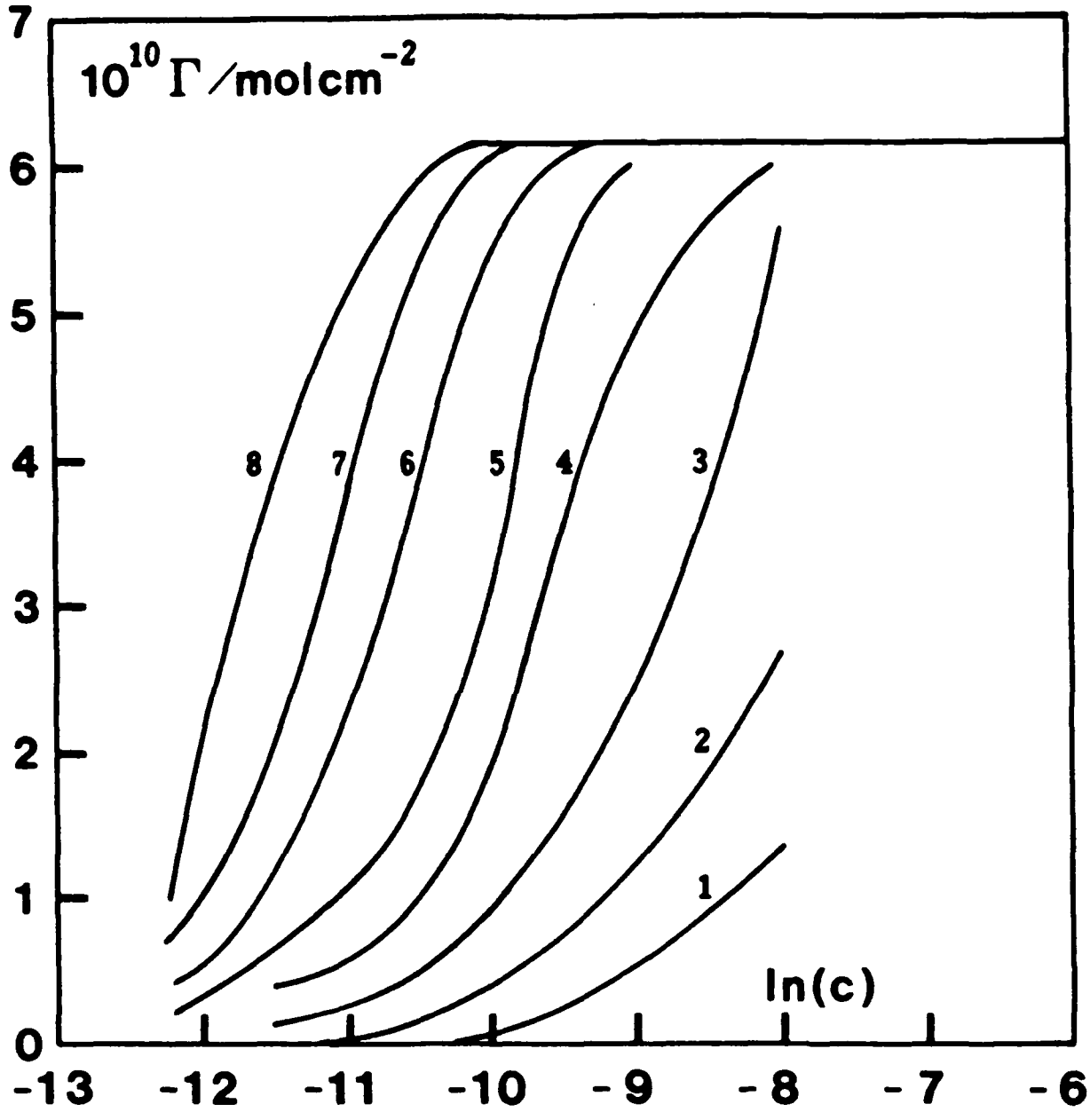

Fig. 7 Adsorption isotherms which have been obtained at the following electrode potentials: (1) -0.45 V; (2) -0.40 V; (3) -0.35 V; (4) -0.30 V; (5) -0.25 V; (6) -0.20 V; (7) -0.15 V; (8) -0.10 V. C is the bulk pyridine concentration.

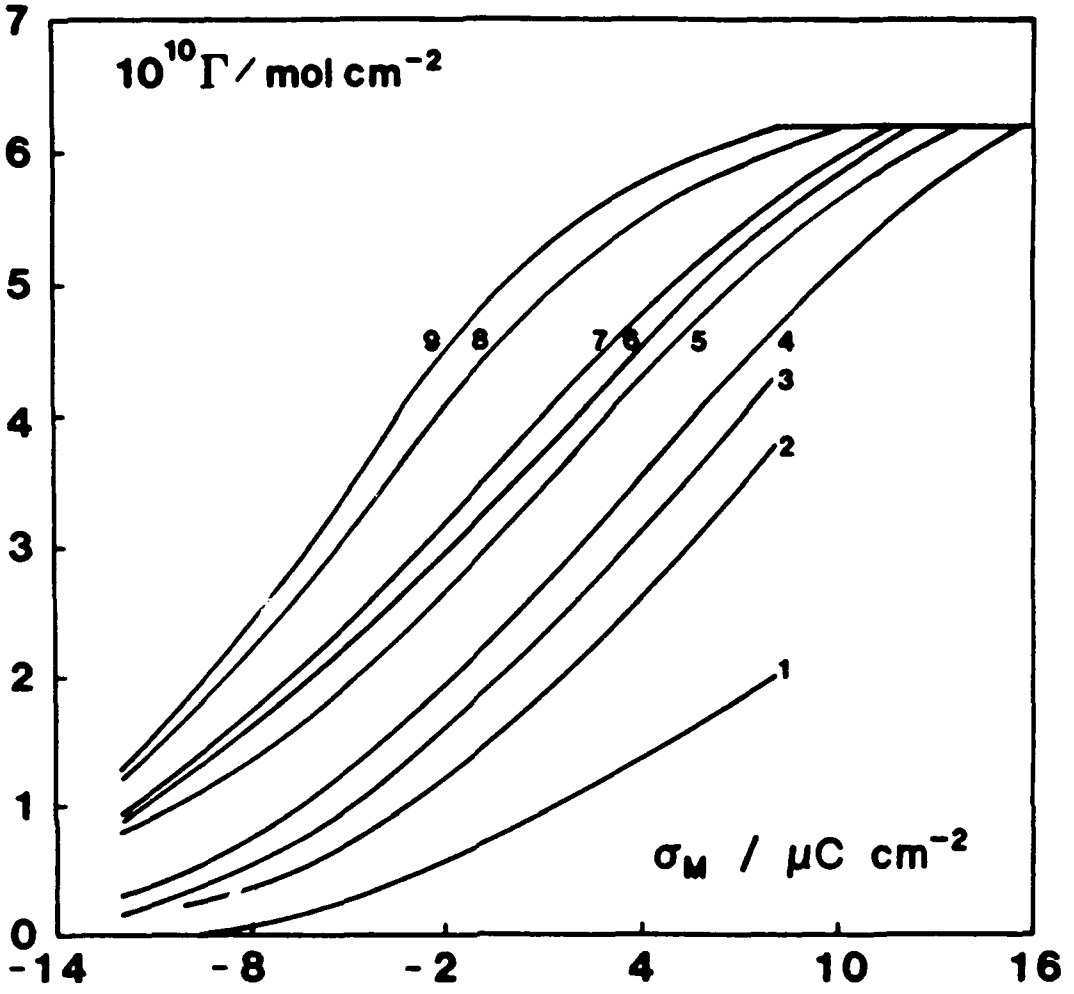

Fig. 8 Surface concentrations - electrode charge density curves obtained for the following bulk pyridine concentrations: (1) 2 x 10^{-6} M; (2) 5 x 10^{-6} M; (3) 7 x 10^{-6} M; (4) 10^{-5} M; (5) 3 x 10^{-5} M (6) 7 x 10^{-5} M; (7) 10^{-4} M; (8) 3 x 10^{-4} M; (9) 6 x 10^{-4} M.

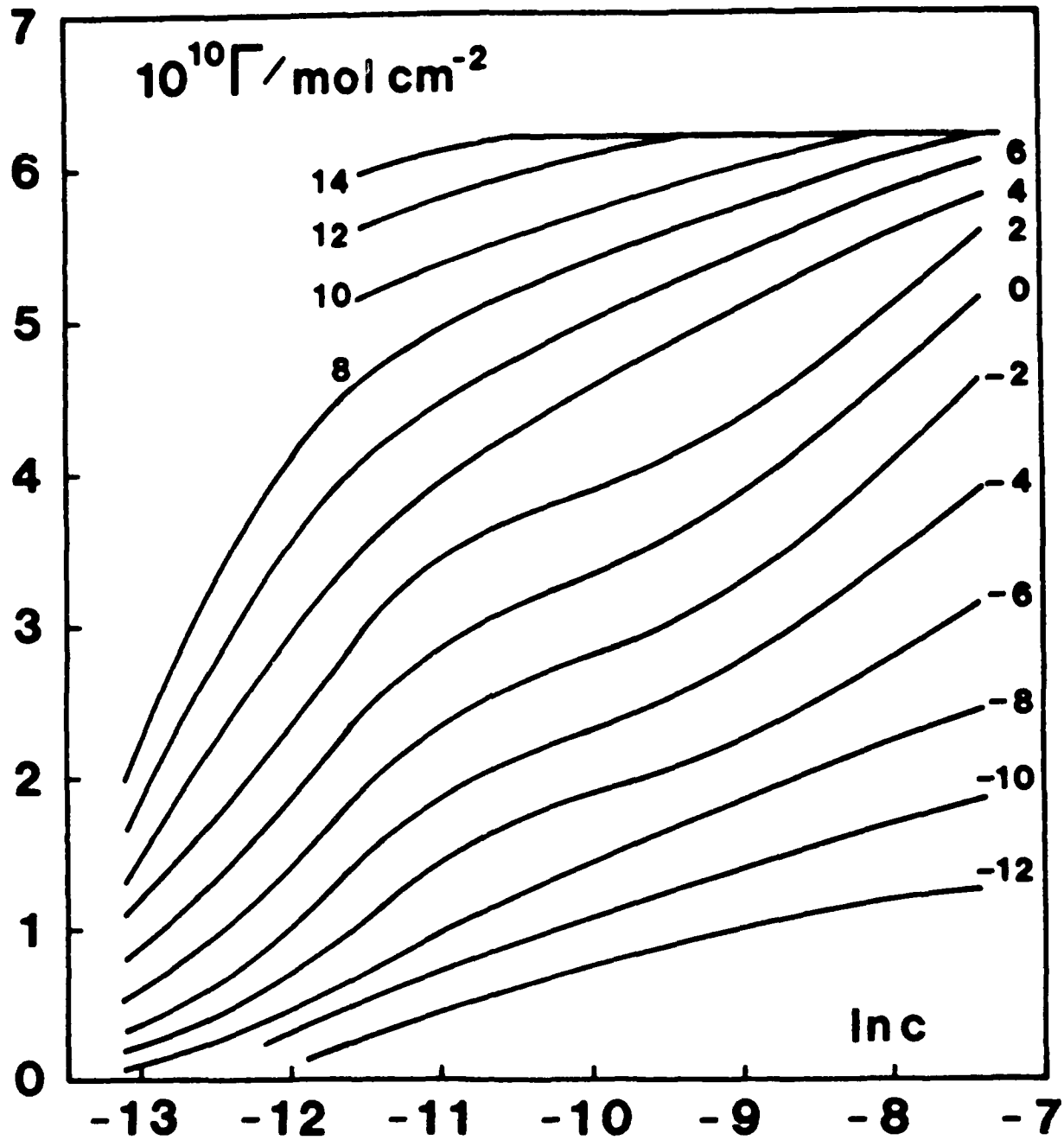

Fig. 9 Adsorption isotherms determined at constant charge densities, the values of which in $\mu C\ cm^{-2}$ is indicated at the corresponding curve.

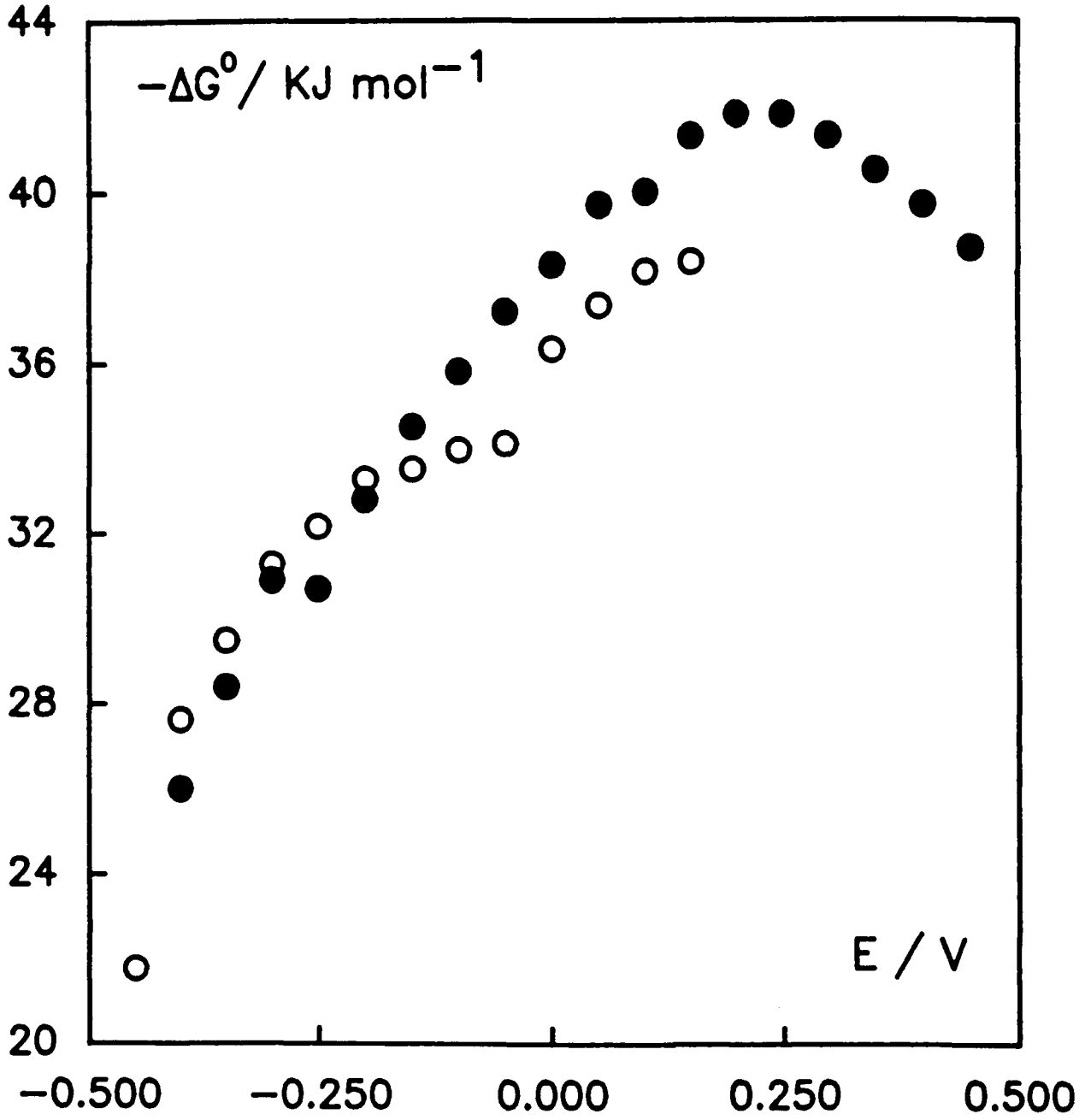

Fig. 10 Plot of ΔG° versus E as determined from the Henry's Law isotherm, filled circles, and from a fit to the equation of the Frumkin isotherm - open circles.

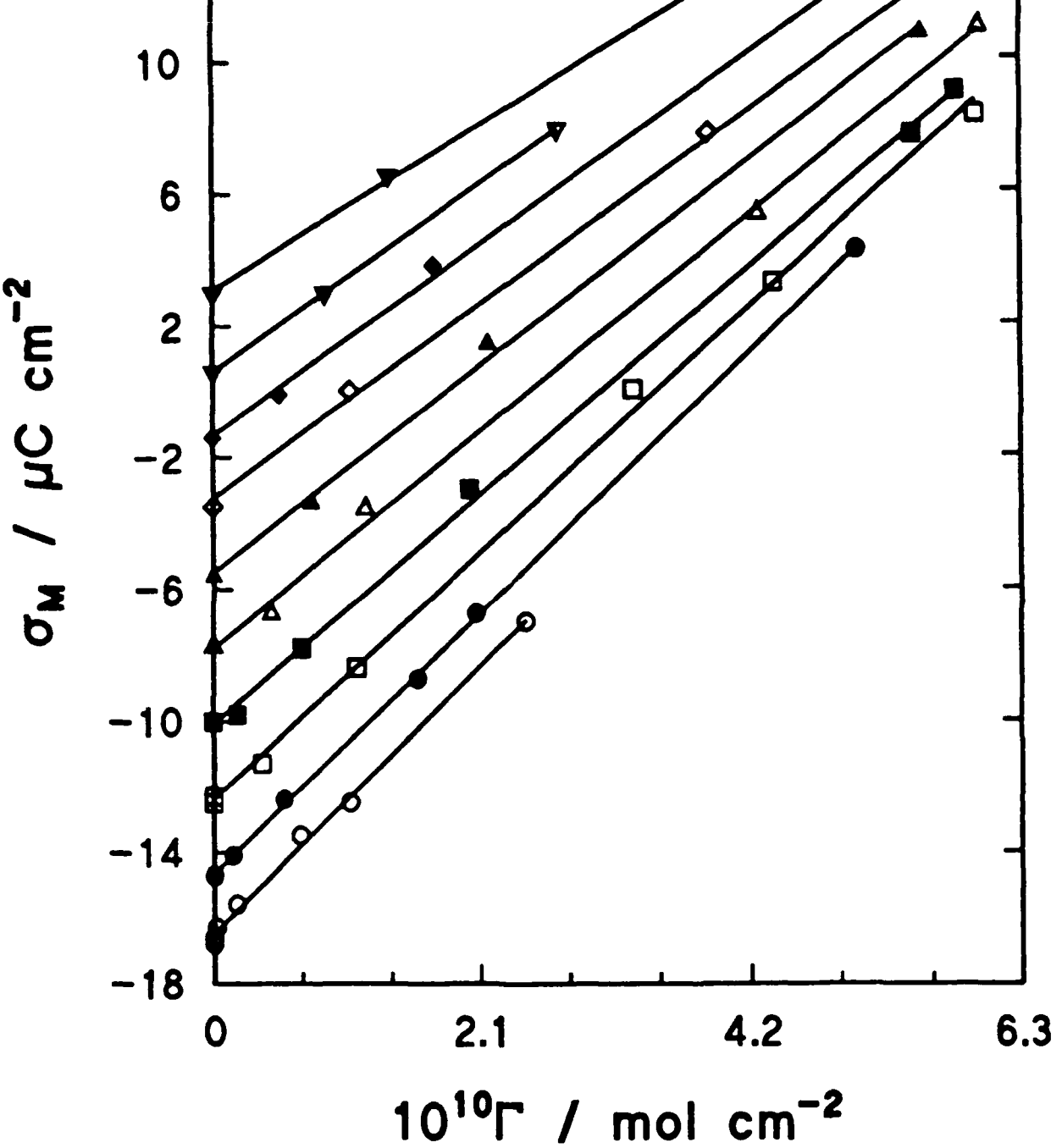

Fig. 11 Plots of σ_M versus Γ at constant E. (○) -0.40 V; (●) -0.30 V; (□) -0.25 V; (■) -0.20 V; (△) -0.15 V; (▲) -0.10 V; (◊) -0.05 V; (♦) 0 V; (▽) +0.05 V; (▼) +0.10 V.

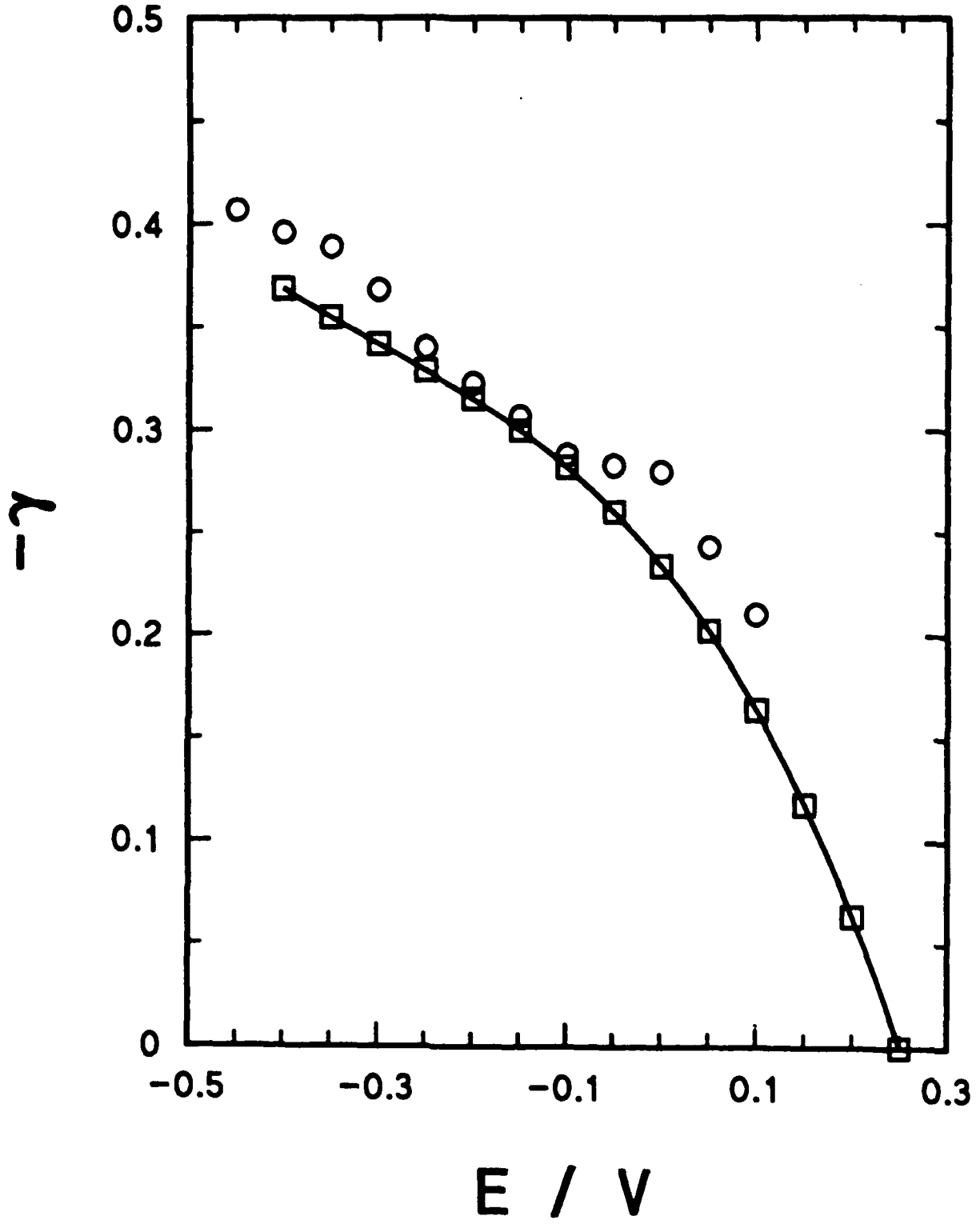

Fig. 12 Comparison of the electrosorption valencies determined from (O), the slopes of the σ_M versus Γ plots, and (□) by numerical differentiation of the ΔG^* vs. E curve corresponding to Henry's Law.

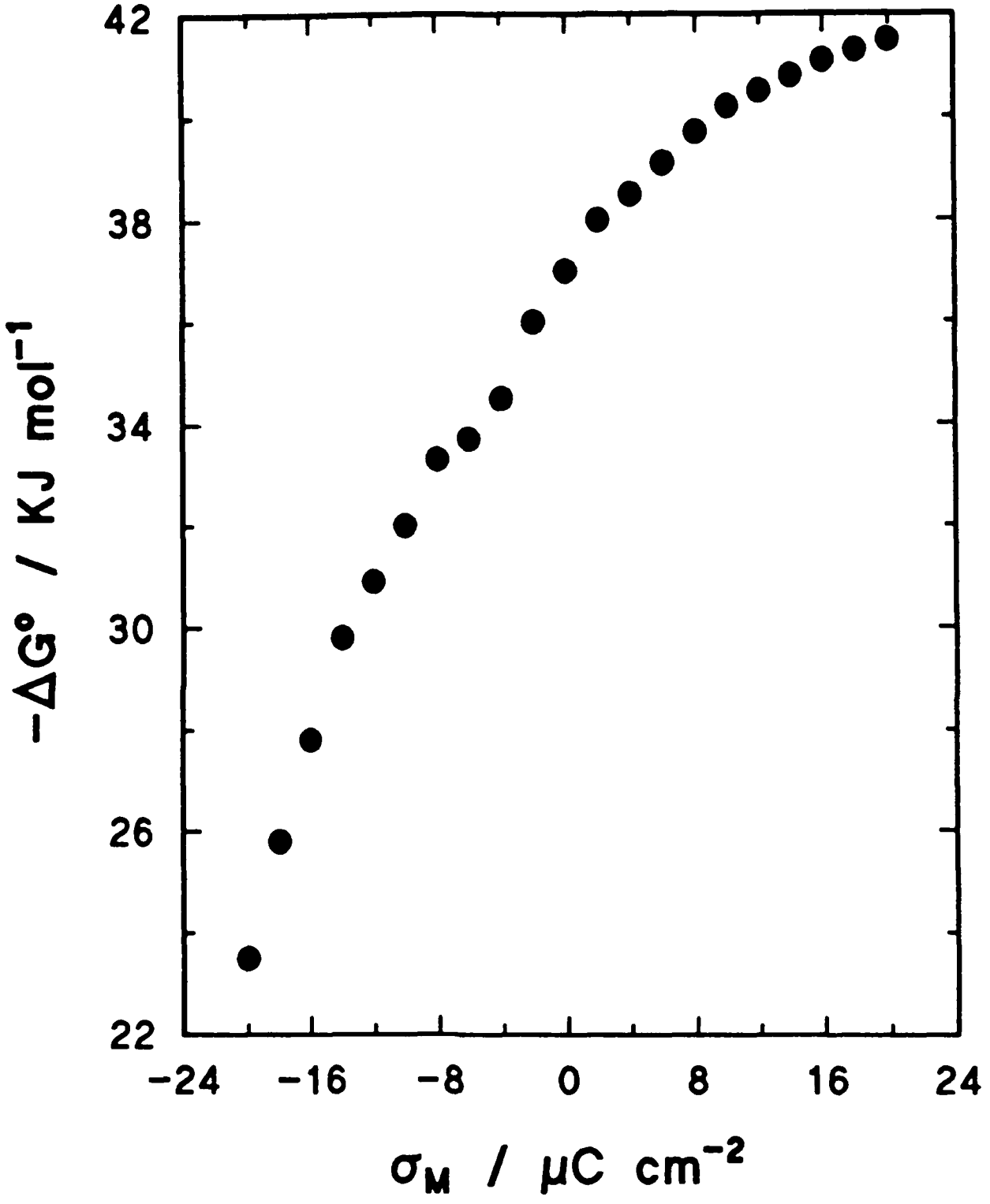

Fig. 13 Plot of ΔG° versus σ_M determined from the Henry's Law isotherm.

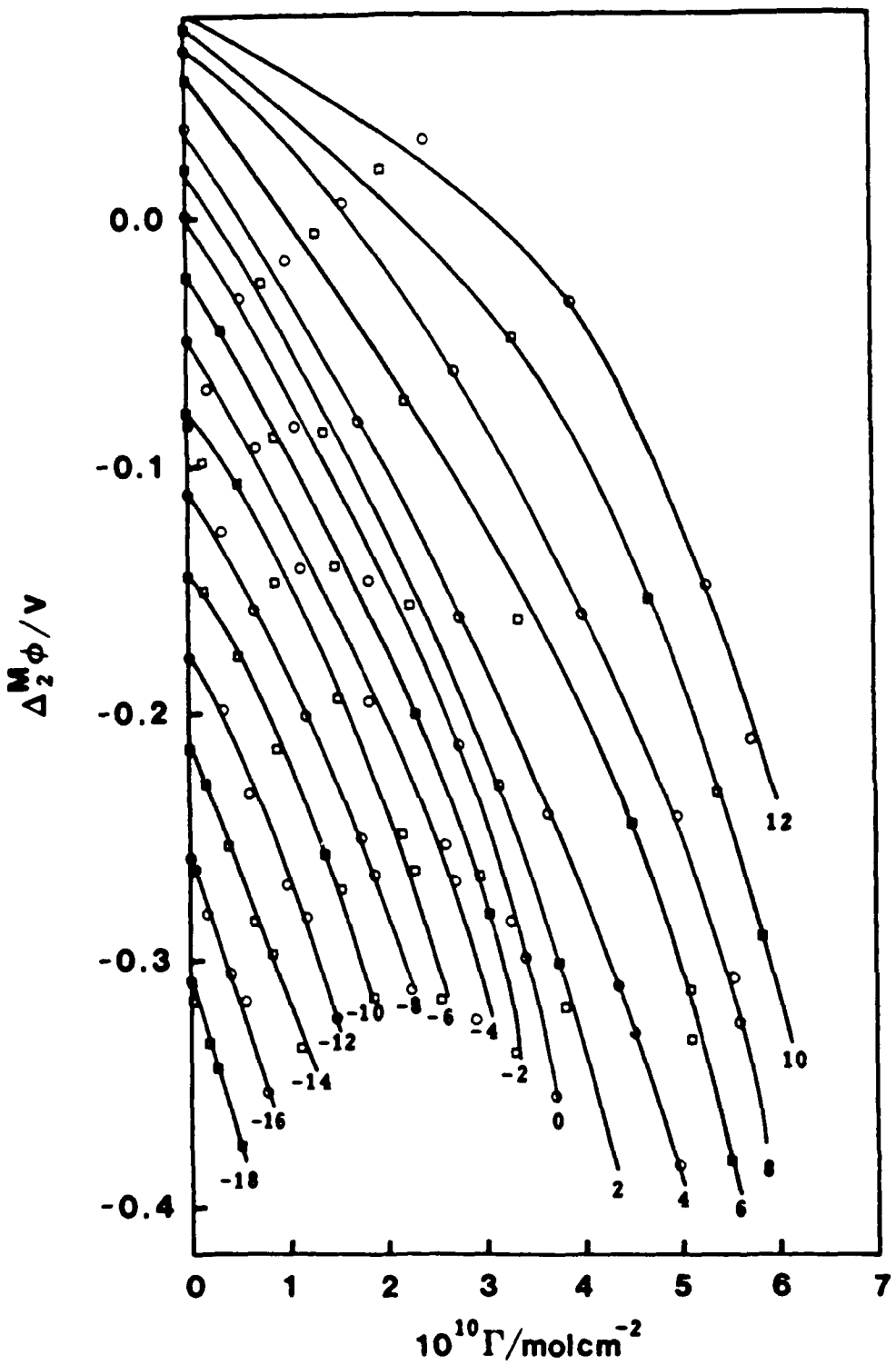

Fig. 14 Plot of $\Delta_2^M\phi$ versus Γ for the various charge densities indicated.

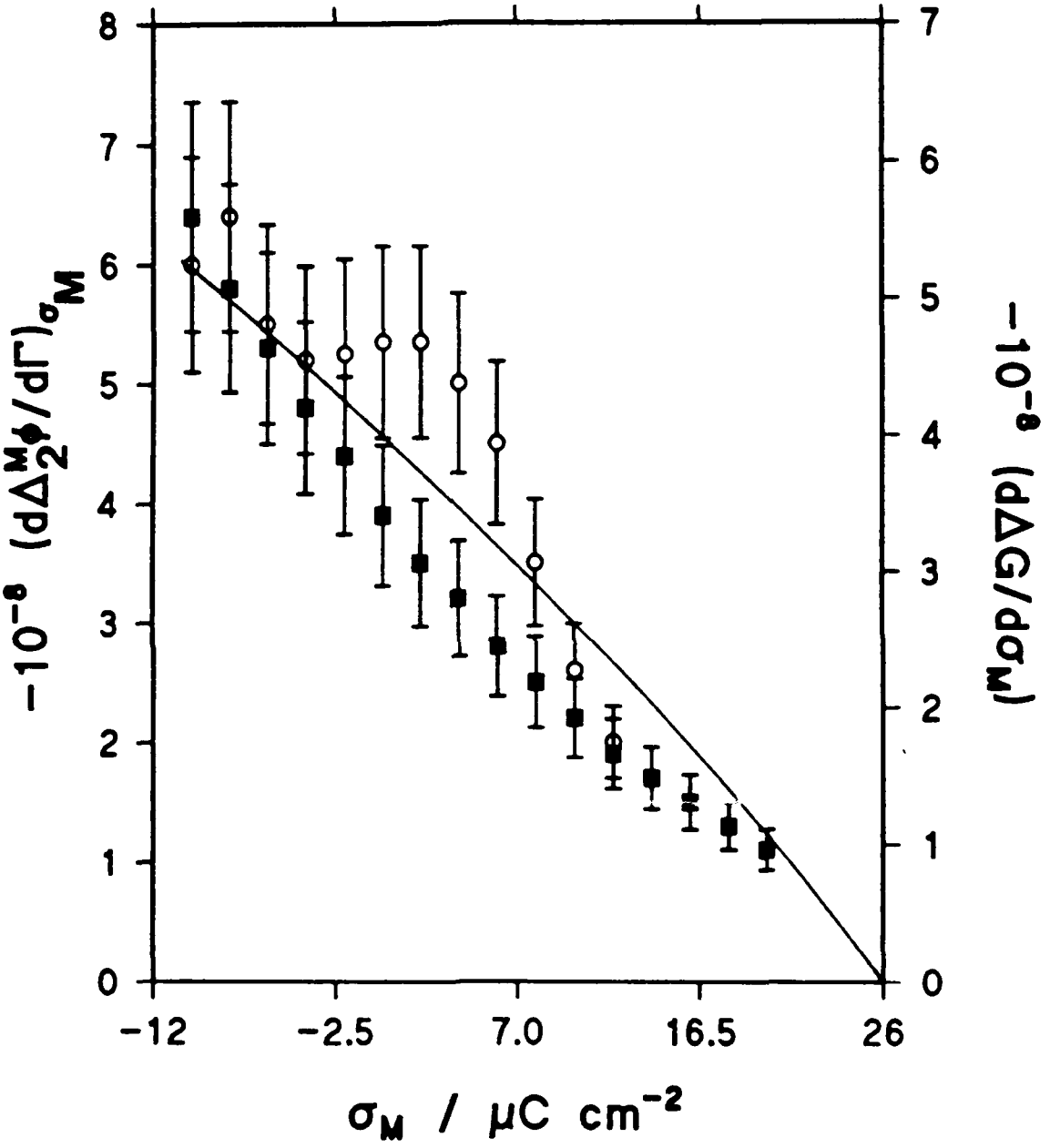

Fig. 15 Comparison of the dependence of $(\partial\Delta_2{}^M\phi/\partial\Gamma)\sigma_M$ on the charge density determined from the initial slopes of the plots in Fig. 14, open circles, and by the numerical differentiation of the Gibbs energy with respect to the electrode charge density, filled squares.

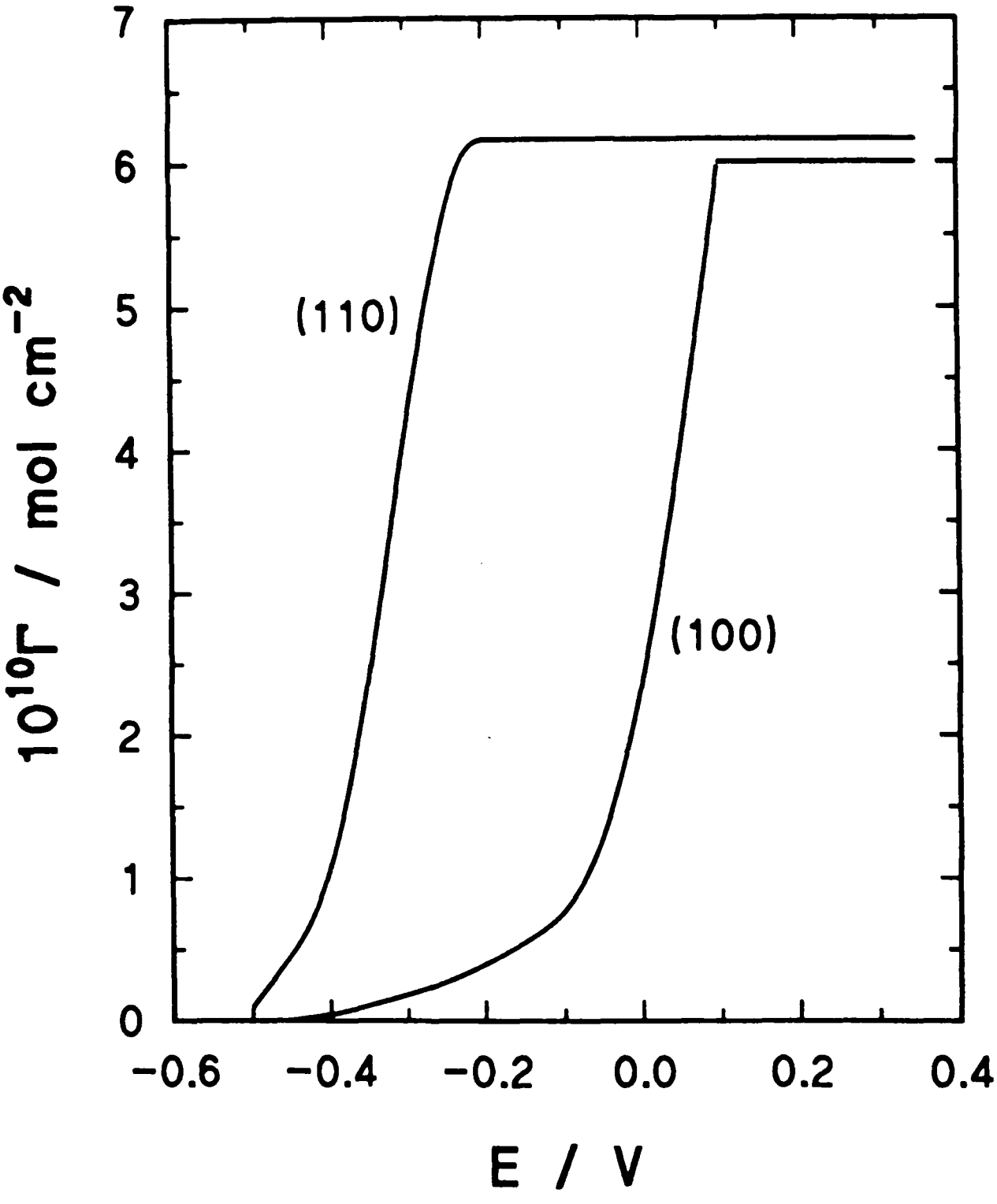

Fig. 16 Comparison of the isotherms for pyridine adsorption at Au(110) and Au(1

surfaces from 10^{-4} M pyridine solution.

TECHNICAL REPORT DISTRIBUTION LIST - GENERAL

Office of Naval Research (2)
Chemistry Division, Code 1113
800 North Quincy Street
Arlington, Virginia 22217-5000

Dr. Robert Green, Director (1)
Chemistry Division, Code 385
Naval Weapons Center
China Lake, CA 93555-6001

Commanding Officer (1)
Naval Weapons Support Center
Dr. Bernard E. Douda
Crane, Indiana 47522-5050

Chief of Naval Research (1)
Special Assistant for Marine Corps Matters
Code 00MC
800 North Quincy Street
Arlington, VA 22217-5000

Dr. Richard W. Drisko (1)
Naval Civil Engineering Laboratory
Code L52
Port Hueneme, CA 93043

Dr. Bernadette Eichinger (1)
Naval Ship Systems Engineering Station
Code 053
Philadelphia Naval Base
Philadelphia, PA 19112

David Taylor Research Center (1)
Dr. Eugene C. Fischer
Annapolis, MD 21402-5067

Dr. Sachio Yamamoto (1)
Naval Ocean Systems Center
Code 52
San Diego, CA 92152-5000

Dr. James S. Murday (1)
Chemistry Division, Code 6100
Naval Research Laboratory
Washington, D.C. 20375-5000

Dr. Harold H. Singerman (1)
David Taylor Research Center
Code 283
Annapolis, MD 21402-5067

Defence Technical Information Center (2)
Building 5
Cameron Station
Alexandria, VA
U.S.A. 22314

ENCLOSURE(2)